Eur Biophys J (2011) 40:247–257
DOI 10.1007/s00249-010-0642-7

ORIGINAL PAPER

Biomembrane force probe investigation of RNA dissociation

Christopher Brampton · Omar Wahab · Matthew R. Batchelor · Stephanie Allen · Philip M. Williams

Received: 13 August 2010 / Revised: 13 October 2010 / Accepted: 10 November 2010 / Published online: 25 November 2010

Abstract Investigations into the energy pathways of biomolecular interactions by use of dynamic force spectroscopy are limited by the range of loading rates accessible with a single technique. In the work discussed in this paper, this range has been extended for a previously studied system by using the biomembrane force probe (BFP). This work builds on our previous single-molecule atomic force microscopy (AFM) study of the dissociation of a bulge-motif-containing RNA complex. The disparity observed, at high loading rates, between the dissociation of a 12-base pair complex with and without a central three-base pair bulge was not observed at low rates. This suggests that the two species share a similar outer barrier to dissociation and that inclusion of the bulge motif creates an additional barrier at a distance closer to the bound state. Experiments performed in different buffer environments yielded similar results. The results, when combined with those of previous studies, suggest that the shared outer barrier to dissociation is that due to a rearrangement and fraying of the ends of the helix.

Keywords DFS · BFP · AFM · RNA · Dynamic force spectroscopy · Biomembrane force probe

C. Brampton · O. Wahab · M. R. Batchelor · S. Allen · P. M. Williams (✉)
Laboratory of Biophysics and Surface Analysis, School of Pharmacy, University of Nottingham, Nottingham NG7 2RD, UK
e-mail: phil.williams@nottingham.ac.uk
URL: http://www.nottingham.ac.uk/LBSA

Introduction

RNA is a key element in many cellular processes, providing both a medium for information transfer in transcription, and functional activity for processing through RNA-based enzymes (Guerriertakada and Altman 1984). The function of a *ribozyme* is related to its structure and this, in turn, is depends on its sequence. Unlike proteins, which have the same linkage of sequence–structure–function but fold cooperatively and often through no intermediates, large RNA molecules can assemble as a hierarchy of independent secondary structure motifs, for example hairpins, bulges, loops, and double helices. The interaction of small RNAs of a few tens of nucleotides is also central to the function of siRNA and microRNA. As with proteins, single-molecule force-induced unfolding studies offer a way to probe the relationship of an RNA molecule structure with its kinetic (mechanical) stability. Such dynamic force spectroscopy (DFS) measurements provide a view of the energy barriers to dissociation/unfolding along a reaction coordinate, and thereby add structural detail to the processing (nuclear export, for example) and function (DNA binding, for example) of the molecule.

DFS is an experimental approach used to study the location and relative magnitude of energy barriers and transitions states along a dissociation pathway induced by force (Evans and Ritchie 1997; Evans and Williams 2001; Williams et al. 2000). By applying stress to a molecular bond at a known rate of force-loading and measuring the force at which the complex dissociates the lifetime of the bond under the force is determined. The dependence of the bond lifetime on force provides a measure of the distance along the unbonding coordinate of the transition state. The lifetime of the bond under zero force can also be

extrapolated. Importantly, because the transition state energy's susceptibility to force, and consequently the dissociation rate, depends on the displacement of the transition state, different levels of force can be used to reveal the presence of multiple transition states. The first DFS study of the streptavidin–biotin interaction, for instance, revealed two transition states (Merkel et al. 1999). Their presence was confirmed through computational and subsequent DFS studies (Galligan et al. 2001; Moore et al. 1998, 1999; Patel et al. 2004; Williams 2006; Williams et al. 2000). DFS has been used to study both DNA and RNA duplexes. Using AFM, Strunz et al. studied the dissociation of DNA duplexes of varying length (a 10mer with 60% GC content, a 20mer with 55% GC content, and a 30mer of 60% GC content) and revealed, as expected, a linear relationship between the displacement of the transition state and an exponential relationship between the extrapolated force-free dissociation rate and the duplex length (Grange et al. 2001; Strunz et al. 1999). The authors later extended their studies to probe the temperature dependence of duplex stability under force (Schumakovitch et al. 2002). Our AFM DFS studies of poly(A)-containing DNA d(CGCAA AAAAGCG) revealed similar dissociation forces to those of Strunz but indicated a different transition state location of 0.6 nm compared with the 1.5 nm predicted (Pope et al. 2001). Combining these DFS data with results from thermal melting studies enabled us to predict an average dissociation energy of approximately 1.7 k_BT and a rate constant (kinetic prefactor) of the order of 10^6 s^{-1} for each DNA base pair, similar to that suggested previously (Craig et al. 1971). We obtained similar results when studying the RNA duplex of the same sequence; a barrier location of 0.7 nm, average dissociation free energy per RNA base pair of 1.1 k_BT, and kinetic prefactor of 10^6 s^{-1} (Green et al. 2004). In this later study we also probed the effect on the dissociation kinetics of introducing a three nucleotide –UCU– bulge in one strand. DFS still revealed a single transition state but at a displacement of 0.4 nm and lower in energy. We suggested that the addition of the bulge to the duplex had introduced a new transition state into the forced-dissociation energy landscape and that the original 0.7 nm barrier was still present but not seen. This inability to see both transition states in the dynamic force spectrum was attributed to the limited range of force-loading rates available to the AFM.

The BFP is a specialist instrument that can provide access to loading rates that are unattainable to the more commonly used AFM and optical trap approaches (Evans et al. 1995). The spring constant of the probe in the BFP is much lower than that of an AFM cantilever, ranging from 10^{-2} to 10^{1} pN nm^{-1} (Gourier et al. 2008), and, unlike an AFM cantilever, the BFP spring constant can be altered straightforwardly in situ to any value within this range. When coupled with the retraction velocities available by use of piezoelectric actuators, the loading rates accessible to the BFP cover over five orders of magnitude through traditional pipette manipulation (10^{-1} to 10^{5} pN s^{-1}), and can be arbitrarily low when aspiration pressure control is used (although thermal drift then dominates). The biomembrane force probe has been used previously for measurement of a variety of single and multiple ligand–receptor unbinding forces (Bayas et al. 2006; Chen et al. 2008a, 2008b; Evans 1998; Evans et al. 2001, 2002, 2004, 2005, 2010; Heinrich et al. 2005; Kinoshita et al. 2010; Merkel et al. 1999; Perret et al. 2004). We believe this is the first time the BFP has been used to study oligonucleotide duplexes.

We have used the BFP to study the dissociation of the RNA duplex with and without the bulge to complement the earlier AFM study and test and extend the conclusions drawn previously.

Materials and methods

Unless stated otherwise, all chemicals were obtained from Sigma–Aldrich (Poole, UK). The biotinylated RNA samples were synthesized by Eurogentec (Copenhagen, Denmark) on a controlled porosity glass support system using the method developed by Sinha et al. (1984). The sequences were:

12-mer	CGCAAAAAACGC-biotin	(ss12-mer1)
	biotin-GCGUUUUUUGCG	(ss12-mer2)
12-merB	CGCAAA**UCU**AAACGC-biotin	(ss15-mer)
	biotin-GCGUUUUUUGCG	(ss12-mer2)

The two complexes differ by the addition of the trinucleotide -**UCU**- at the centre of one of the RNA strands. All procedures involving RNA samples were carried out using sterile techniques to minimise loss by ribonuclease contamination: all work surfaces were wiped with an RNase inhibitor; solutions were prepared using deionised and autoclaved water (Elga, UK) and filtered through sterile 0.2 μm syringe filters (Sartorius, Germany); sterilised, disposable plastic-ware was used where possible.

Biomembrane force probe

The BFP used is similar to that described by Evans et al. (1995) and uses a red blood cell (RBC) as its force transducer. The RBC is pressurised by suction into a glass micropipette, and a microscopic glass bead chemically attached to the pole of the RBC serves as the "probe" surface to which the molecules of interest are tethered. A "test" bead modified with the interacting partner molecule is held in a

second micropipette co-axially aligned and opposed to the probe. The precise displacement of the test bead is achieved by mounting this second micropipette on a single-axis 38 μm piezoelectric actuator with feedback control (PI, Karlsruhe, Germany). Two glass coverslips form the top and bottom of the BFP chamber and the micropipettes access the chamber horizontally from the open sides (Merkel et al. 1999). The whole apparatus is set up on the stage of an inverted optical microscope (Eclipse TE 2000; Nikon UK).

Micropipettes were prepared by pulling borosilicate glass tubes (100 mm long, 1.0 mm outer diameter, 0.75 mm inner diameter; Sutter Instruments, UK) using a P97 pipette puller (Sutter Instruments). A microforge (Narishige International, UK), was then used to mill the ends of the pipettes leaving them squared-off and with the required inner dimension. Before experiments, the chamber and micropipettes were filled with a 200 mOsm L^{-1} (1 Osm = 1 mol of osmosis-affecting ions) PBS solution containing 0.5% bovine serum albumin (BSA). This solution was left in place for at least 30 min before exchanging it for the measurement buffer. Compacted beads and RBCs were added to separate parts of the chamber floor in ~2 μL quantities. A third "working" micropipette mounted at an angle to the horizontal on a 3D hydraulic manipulator was used to transfer RBCs and beads and prepare the probe. Figure 1 shows an image of the BFP system.

For force calibration, measurements were taken of the radius of the RBC (R_o), the inner radius of the probe micropipette (R_p), and the radius of adhesive contact between the RBC and probe bead (R_b). The pressure on the probe (P) was then adjusted to set and maintain a given force constant (k_f), by use of Eq. 1 (Simson et al. 1998):

$$k_f = \frac{RpP}{2\left(1-\frac{R_p}{R_o}\right)\ln\left(\frac{4R_o^2}{R_bR_p}\right) - \left(1-\frac{R_p}{4R_o}-\frac{3R_b^2}{8R_o^2}+\frac{R_b^2}{R_o^2}\right)} \qquad (1)$$

This equation gives probe stiffness values significantly higher than when using the equation of Evans et al. (1995), and has recently been shown to be valid for the small deformations/forces encountered here (Heinrich and Ounkomol 2007). During a computer-programmed measurement cycle the test bead is driven into contact with the probe bead, the beads are held in contact at a fixed deflection for a fixed duration and then the test bead is retracted at a set rate. The deflection of the RBC is detected throughout by monitoring the change in position of the diffraction edge between probe bead and RBC by use of a fast frame-rate camera (SensiCam, Cooke, MI, USA). The camera only views a narrow section along the aligned RBC/probe bead/test bead system axis, and a parabola is fit to the dip in intensity associated with the diffraction edge. Each pixel in the image has a size of roughly 40 nm, but by this method the centre of the parabola and, thereby, the deflection of the RBC, can be tracked with a resolution of ~5 nm. The measurement cycle was repeated many hundreds of times and the resulting deflection versus time plots were collected and analysed. Experiments were performed over a wide range of different loading rates to provide as much detail of the dynamic force spectrum as possible.

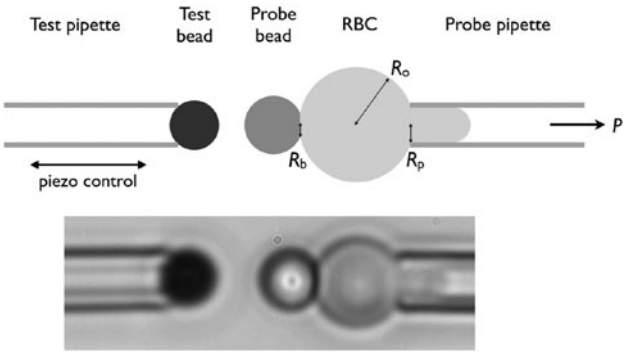

Fig. 1 Schematic diagram and optical image of the BFP. There are two *horizontal*, co-axially aligned pipettes: the one to the *right* aspirates with pressure P the "probe" being a red blood cell, radius R_o, glued to the probe bead through multiple biotin–streptavidin interactions with a contact radius of R_b; to the *left* the pipette aspirates a test bead directly. A third "working" pipette, not shown, is mounted at an angle and provides a means for transferring beads and setting up the probe. For scale, the inner radius of the probe pipette, R_p, was measured as 0.9 μm

Functionalisation of red blood cells

By using a microcentrifuge to remove the liquid fractions, fresh rabbit red blood cells (from 12 μL of blood) were washed three times with 150 μL coating buffer (sodium carbonate–sodium bicarbonate buffer, 0.1 mol L^{-1}, pH 8.5). The cells were then modified by reaction of the ubiquitous amino groups on the membrane surface with a biotin-containing polymer. A few microlitres of washed, packed RBCs were gently mixed for 30 min in 1 mL of a 3 mg mL^{-1} coating buffer solution of α-biotin-ω-carboxysuccinimidyl ester poly(ethylene glycol)—PEG molecular weight 3,000 Da (NHS–PEG–biotin; Shearwater Polymers, Huntsville, AL, USA). The modified cells were washed a further three times with 150 μL coating buffer before a final wash with the measurement buffer.

Functionalisation of glass beads

Borosilicate glass beads (average diameter ~2 μm; Duke Scientific, USA) were modified with biotin. Streptavidin was then used as a crosslinker to link the beads to the RNA molecules and also, in the case of the probe bead, to a biotinylated RBC. Briefly, the glass beads were cleaned in a boiling solution of aqueous ammonia and hydrogen peroxide (pH 10.9), rinsed with deionised water by

centrifugation, and then treated with mercaptopropyltrimethoxysilane (MPTMS). One 2.5 mg aliquot of these thiol-modified beads was then mixed for 30 min in 1 mL of a 4 mg mL^{-1} PBS solution of α-biotin-ω-maleinimido poly(ethylene glycol)—PEG molecular weight 3,400 Da (Mal–PEG–biotin; Shearwater Polymers). Biotinylated beads were suspended in 1.5 mg mL^{-1} streptavidin for 30 min, rinsed, and stored in PBS before use.

Probe beads require the surface density of RNA molecules to be controlled—the bead needs sufficient RNA to give suitable interaction numbers during experiment and yet have enough unbound streptavidin so that it strongly adheres to the RBC. To this end, streptavidin-coated beads were modified using different concentrations of RNA. Bead aliquots were incubated at room temperature for 2 h in 100 μL of the single-stranded RNA solutions; the concentrations used were 6, 8, 10, and 12 μg mL^{-1}.

Measurement buffers

Two different buffers were used throughout the course of these experiments: phosphate (in PBS) and HEPES. For a correctly working BFP the osmolarity of the measurement buffer must be regulated to maintain the structural integrity and elastic properties of the RBC. If the osmotic potential is too high the RBC shrinks and is insufficiently stiff; if it is too low, the cell will lyse. It has been found that an osmolarity of approximately 200 mOsm L^{-1} is required for a workable BFP. PBS buffer was prepared by diluting the ~300 mOsm L^{-1} solution from a commercial tablet with 50% deionised water. This gave a solution containing 7 mmol L^{-1} phosphate, 91 mmol L^{-1} NaCl, and 1.8 mmol L^{-1} KCl. HEPES buffer of 200 mOsm L^{-1} was prepared using 14 mmol L^{-1} HEPES and 98 mmol L^{-1} NaCl. Both solutions were adjusted to pH 7 and contained 0.1% bovine serum albumen (BSA), which reduces non-specific interactions between the BFP components. To test the effect of magnesium ions on the stability of the bulge-containing complex, experiments were also performed in HEPES buffer with an additional 10 mmol L^{-1} $MgCl_2$.

Results

Collection of data sets

In any batch of measurements, the force curves revealing single-molecule, specific interactions must be separated from those with non-specific or multiple interactions before analysis. An example of a force curve is given in Fig. 2. Unlike the force curves in our previous AFM experiments (Green et al. 2004; Pope et al. 2001), because the spring constant of the RBC is so low, the shape of the force curves recorded using the BFP can appear the same for all types of interaction, be they single-specific, non-specific, or multiple-specific interactions breaking simultaneously. For this reason, our experiments rely on Poisson statistics to ensure that most of the forces measured are due to single-molecule interactions (Williams 2003). In order to do this, the level of non-specific interaction between beads must be insignificantly low; this is achieved by proper choice of surface chemistry and gauged by suitable control experiments. The probability of a force curve revealing any interaction is then set to a low level by controlling the numbers of interacting species on the surface. The small number of curves in which two or more individual break-offs were observed on retraction were discounted. It was found that data collected using very fast retraction velocities were unreliable. Fast rates resulted in low resolution in the all-important adhesive region of the force curve and made it very difficult to detect and reject any undesirable multi-break curves. All data collected at loading rates greater than 5,000 pN s^{-1} were therefore omitted from the final analysis.

Preparation of RNA-modified beads

A series of experiments was performed to gauge the optimum conditions for bead modification with RNA. Beads prepared using 8 μg mL^{-1} biotinylated RNA adhered strongly to RBCs while still giving a hit-rate of interaction of approximately 10%. This hit rate is low enough to ensure that most of the adhesive contacts recorded are due to single-molecule interactions (according to Poisson

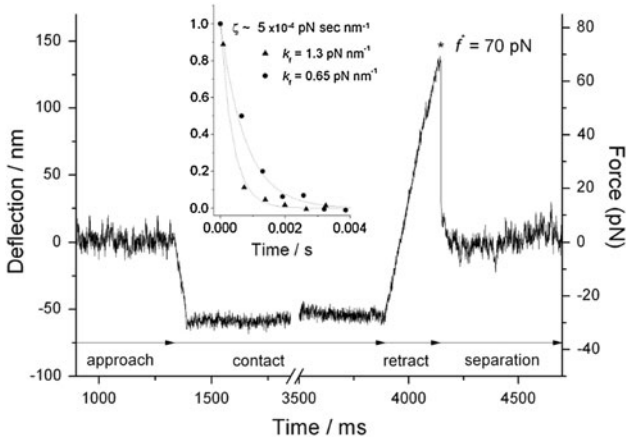

Fig. 2 A typical force curve. The probe was calibrated to give $k = 0.5$ pN nm^{-1}. The piezo moved the beads so they approached at 2,000 nm s^{-1}; contact was made and held for 2.5 s at a deflection of 60 nm (30 pN). The beads were then pulled apart at 1,000 nm s^{-1} ($r_f = 500$ pN s^{-1}). The maximum (adhesive) deflection from the baseline was 139 nm (70 pN)

statistics (Williams 2003)), and yet the numbers were not too few to prohibit the collection of data of statistical relevance within a reasonable timeframe. Most of the data presented were collected using beads prepared using 8 μg mL^{-1} RNA solutions.

Probe stiffness

The elastic stiffness of the RBC was checked by recording its recovery after duplex breakage. Inset in Fig. 2 is a plot of the normalized extension of the RBC after bond rupture for two tests with probes of different elastic stiffness (0.65 and 1.3 pN nm^{-1}) with exponential decays overlaid defined by the time scale ζ/k_f and a common damping coefficient $\zeta = 5 \times 10^{-4}$ pN s nm^{-1} (Evans and Williams 2001). This damping coefficient is an order of magnitude lower than that of an AFM cantilever ($\zeta_{afm} \sim 5 \times 10^{-3}$ pN s nm^{-1}) (Alcaraz et al. 2002; Janovjak et al. 2005; Maali et al. 2005) and reflects the order-of-magnitude smaller dimension of the cell probe compared to a typical AFM lever. This lower damping coefficient of the BFP is of substantial benefit, because the force on the bond due to the hydrodynamic drag of the probe moving through the liquid, $\Delta f = \zeta v$, which is hidden in the measurement, is commensurately lower (at a retraction velocity of 10,000 nm s^{-1} the BFP "misses" a force of 5 pN compared with the AFM of up to 50 pN).

Control experiments

Control experiments were performed to ensure the specificity of the interaction between the complementary RNA strands (Fig. 3 inset). Experiments were performed without modifying the test bead with RNA, i.e. the bead was modified with biotin and streptavidin only. This resulted in the collection of very few curves with an adhesive interaction above the baseline noise level. Furthermore, it was also found that the frequency of interaction could be significantly reduced (below usable levels) by incubating one or other of the RNA-modified beads with an excess of the complementary strand for 40 min before taking measurements. This effectively blocked the sites for strand association between beads.

Force curve analysis

The dissociation force was measured for the selected curves by subtracting the peak deflection from an average or hand-measured baseline and multiplying by the force constant for the system. At least 40 and often several hundred curves were acquired at each pulling rate to give a distribution of dissociation forces. The mode of each distribution, found by using the cumulative distribution

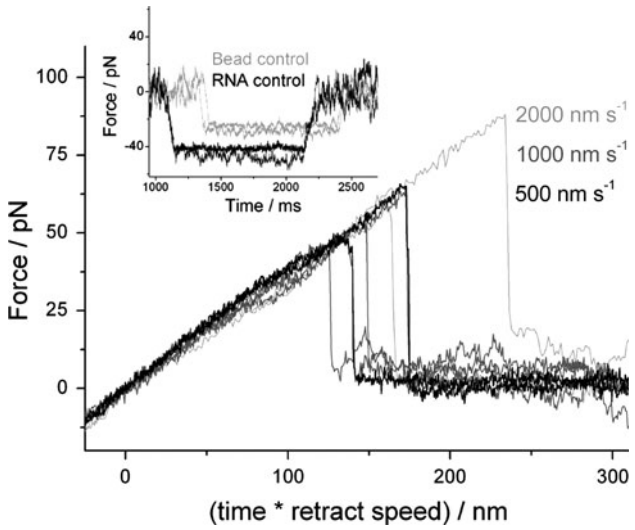

Fig. 3 Example force versus separation (calculated as the product of the time since zero contact force on bead retraction and the retraction velocity) curves acquired at 500, 1,000, and 2,000 nm s^{-1}. The inflexion in the curves at approximately 30 pN is attributed to bead separation. The force ramp is linear in all cases. *Inset* are typical force versus time traces showing no adhesion acquired for the control experiments of RNA-functionalized bead against strepavidin-coated bead (bead control) and RNA-functionalized bead against complementary-RNA bead blocked with excess RNA (RNA control)

method (Williams 2008), was then plotted against the loading rate (r_f), i.e. the dynamic force spectrum, where r_f is simply given by the product of the probe force constant (k_f) and the piezo retraction velocity (v) because, unlike the AFM, the probe force constant is weaker than the molecular linkages (Williams 2008). The linear force loading is demonstrated in Fig. 3, where the force between BFP beads is plotted as a function of time multiplied by retraction speed, i.e. the distance between beads. The loading profile is independent of retraction velocity. The inflexion in the curves at approximately 30 pN is attributed to the separation of the beads. The relationship between the mode adhesion force (f^*) and the loading rate is given in Eq. 2 (Evans 2001; Evans and Ritchie 1997).

$$f^* = f_\beta \ln\left(\frac{r_f}{f_\beta k_{off}}\right) \quad (2)$$

Two variables, f_β and k_{off}, are obtained from a best-fit to the points. The force scale, f_β, is defined as $k_B T/x_\beta$, where x_β is the distance along the dissociation pathway from the bound state to the dominant transition state. The dominant transition state will depend on the loading rate used, because application of an external force to the system distorts the energy pathway and reveals the presence of inner energy barriers. The value of k_{off}, the dissociation rate at zero loading, depends upon the height of each particular energy barrier. By measuring these two values,

parts of the energy landscape for dissociation are revealed. In all the cases shown here a single-energy barrier was revealed over the range of loading rates accessible to the BFP, as indicated by a single slope in the dynamic force spectrum.

The simplest interpretation of force-exponentiated molecular dissociation, with a force-independent transition state(s) and constant kinetic prefactor (force-independent diffusion and energy landscape), through Eq. 2 is used here because it requires fitting of the fewest variables. More complex models of dissociation, for example those proposed by Hummer and Szabo, rely on finding curvature in the semi-logarithmic plot (Dudko et al. 2008; Hummer and Szabo 2003). Such curvature, however, can be attributed to several unrelated properties—a force-dependent transition state, a smooth transition state, force-dependent diffusion (Williams 2008). The data presented are adequately described by Eq. 2, and fitting of further variables here is unwarranted and invalid. Comparison of each measured force histogram with the distribution predicted from the dynamic force spectrum serves as a useful test of the quality of the measurements.

Dissociation of the 12-mer (fully complementary) duplex

Measurements of unfolding forces were taken for the 12mer complex under two different buffer environments across loading rates from 250 to 5000 pN s^{-1}. The results of these, and the rest of the dynamic force measurements, are given in Table 1. In both PBS and HEPES environments a single barrier to dissociation across the loading range was observed (Fig. 4a). The force scales (f_β) were the same within experimental error, and indicate that the distance to the energy barrier was 0.6 nm (0.52 nm $< x_\beta <$ 0.65 nm measured in PBS; 0.55 nm $< x_\beta <$ 0.88 nm measured in HEPES). The calculated dissociation rate under zero applied force (k_{off}) was also the same at 0.3 s^{-1} (0.3 and 0.2 s^{-1} for PBS and HEPES buffers, respectively).

Dissociation of the 12-merB (bulge-motif) duplex

Insertion of three additional ribonucleotides in the centre of one strand causes the formation of a duplex with a bulge. The dynamic force spectrum for the dissociation of this complex in PBS gave mode-rupture forces between 19 and 50 pN for measurements at loading rates of 75 to 5,000 pN s^{-1}, and a resulting force scale of 8.5 pN. In HEPES, similar results were again achieved with forces of 15 and 45 pN for rates of 18 and 5000 pN s^{-1}, respectively, and a force scale of 5.8 pN similar to that measured for the 12mer (Fig. 4b, open symbols). The barrier to dissociation at these rates was therefore located at a distance of approximately 0.6 nm (0.43 nm $< x_\beta <$ 0.56 nm measured in PBS; 0.65 nm $< x_\beta <$ 0.78 nm measured in HEPES). The effect of buffer on the barrier location was more pronounced for the 12merB than for the 12mer.

Dissociation of the 12merB (bulge-motif) duplex in the presence of magnesium

Additional force spectroscopy measurements were collected with magnesium ions (10 mmol L^{-1} $MgCl_2$) added to the HEPES buffered solution (Fig. 4b, closed symbols). No significant change in the resultant force scale (6.9 pN) or unbinding rate (0.3 s^{-1}) was observed compared with measurements without magnesium ions.

Discussion

This study is the first example of use of the biomembrane force probe for studies of the dissociation of a nucleic acid

Table 1 The force scale (f_β), dissociation rate (k_{off}), and distance to energy barrier (x_β) for the two RNA duplexes under different experimental conditions

System	f_β (pN)	k_{off} (s^{-1})	x_β (nm)
12mer (PBS)	7.1 ± 0.8	0.3 ($10^{-0.5 \pm 0.4}$)	0.58 (0.52–0.65)
12mer (HEPES)	6.1 ± 1.4	0.2 ($10^{-0.7 \pm 0.1}$)	0.67 (0.55–0.88)
12mer (Tris) AFM[a]	5.8 ± 0.3	0.4 ($10^{-0.4 \pm 0.2}$)	0.71 (0.67–0.75)
12merB (PBS)	8.5 ± 1.1	1.0 ($10^{0.0 \pm 0.9}$)	0.48 (0.43–0.56)
12merB (HEPES)	5.8 ± 0.5	0.3 ($10^{-0.6 \pm 0.2}$)	0.71 (0.65–0.78)
12merB (HEPES + Mg)	6.9 ± 0.5	0.3 ($10^{-0.6 \pm 0.3}$)	0.60 (0.56–0.64)
12merB (Tris) AFM[a]	10.8 ± 1.1	7.9 ($10^{0.9 \pm 0.2}$)	0.38 (0.35–0.42)

Standard error ranges for f_β, k_{off}, and x_β were taken from the regression statistics and apply to the least-squares fitting

[a] The AFM data included for comparison are taken from Green et al. (2004)

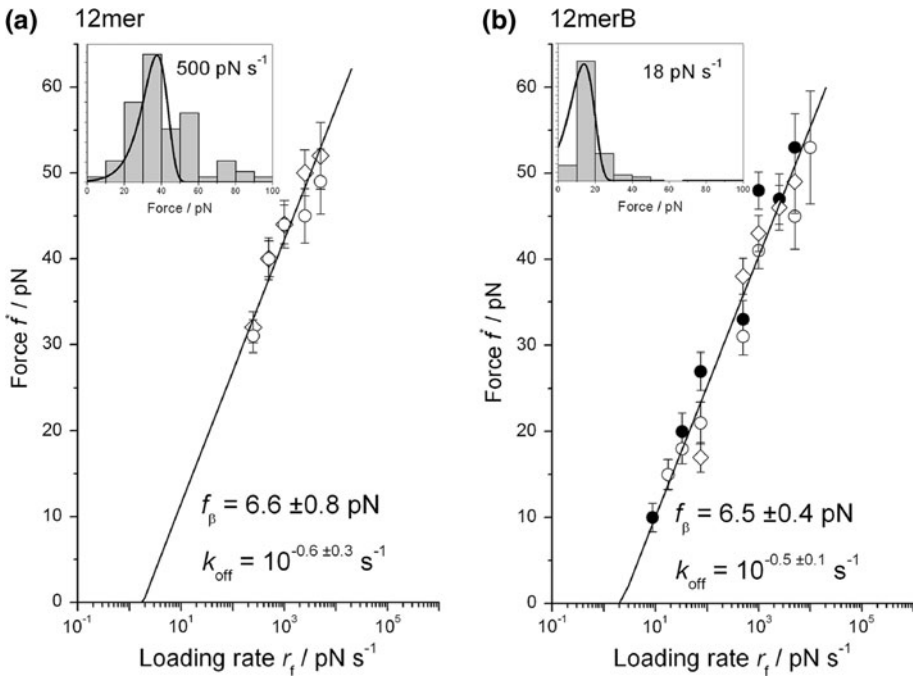

Fig. 4 Dynamic force spectrum for the dissociation of the **a** 12mer duplex and the **b** 12merB duplex measured in PBS (*diamonds*) and HEPES (*circles*) buffers. **a** The 12mer duplex. The *solid line* represents the predicted dynamic force spectrum for breakage of a single bond characterized by a force scale $f_\beta = 6.6$ pN ($x_\beta = 0.6$ nm) and a dissociation rate $k_{off} = 0.3$ s^{-1}. Representative force histogram at 500 pN s^{-1} is *inset* (*x-axis* = adhesion force in pN, *y-axis* = frequency). **b** The 12merB duplex. Dynamic force spectrum for the dissociation of the 12merB duplex in PBS and HEPES buffers with (*closed symbols*) and without (*open symbols*) magnesium. The *solid line* represents the predicted dynamic force spectrum for breakage of a single bond characterized by a force scale $f_\beta = 6.5$ pN ($x_\beta = 0.6$ nm) and a dissociation rate $k_{off} = 0.3$ s^{-1}. Representative force histogram at 18 pN s^{-1} is *inset* (*x-axis* = adhesion force in pN, *y-axis* = frequency)

duplex. By combining the results presented here with those from our previous study using AFM, a more complete view of the energy landscape for dissociation of 12mer RNA duplexes with and without a central three-base bulge-motif has been obtained.

The dynamic force spectra of the dissociation of the fully complementary 12mer in PBS and HEPES buffers revealed identical (within error) off-rates and force scales, similar to those measured previously for this RNA duplex in Tris buffer using the AFM (Green et al. 2004). The force scale of 6.6 pN also matches the 7 pN measured by AFM for dissociation of a 12-mer of DNA with the nucleotide sequence corresponding to that measured here (Pope et al. 2001). The force scale corresponds to a transition state displaced by only 0.6 nm, a fraction of the 4 nm unstretched length of the duplex. It is interesting to note that these force scales of approximately 7 pN recorded here and elsewhere for this poly(A)-tract RNA (DNA) duplex differ substantially from the 3.2 pN predicted from measurements of non-poly(A) tract DNA (Strunz et al. 1999). We believe these differences mirror the different helix–coil transition behaviour of central CG-containing duplexes (Braunlin and Bloomfield 1991; Porschke 1971; Porschke and Eigen 1971; Porschke et al. 1973). These data suggest that the dissociation barrier measured by both the AFM and BFP for the 12mer RNA sequence and of the DNA equivalent is characterized by a force scale of 6.6 pN ($x_\beta \approx 0.6$ nm) and an off-rate of 0.3 s^{-1}.

In their studies of DNA with 55 to 60% GC content, Strunz et al. found a linear correlation between the number of base pairs in the double strand, n, and the distance to the measured energy barrier of $x_\beta \approx (0.7 + 0.07n)$ nm (Strunz et al. 1999). The origins and significance of the 0.7 ± 0.3 nm offset in distance was unclear. It is believed that the rate-limiting step in duplex formation is the creation of a critical nucleus, and for strand dissociation it is internal GC residues that provide this rate-limiting step after fraying of the strand ends (Braunlin and Bloomfield 1991; Porschke et al. 1973; Williams et al. 1989). Molecular dynamics simulations (unpublished) also suggest that partial melting of the helix occurs, forming "denaturation bubbles" between GC residues (Harris et al. 2005). In the A_6-tract RNA system studied here (and the DNA system studied previously (Pope et al. 2001)) there are no central GC residues and therefore no critical rate-limiting GC nucleus. We have shown that the displacement of the energy barrier measured for the A_6-tract RNA and DNA with CGC end caps is similar to the 0.7 nm offset measured

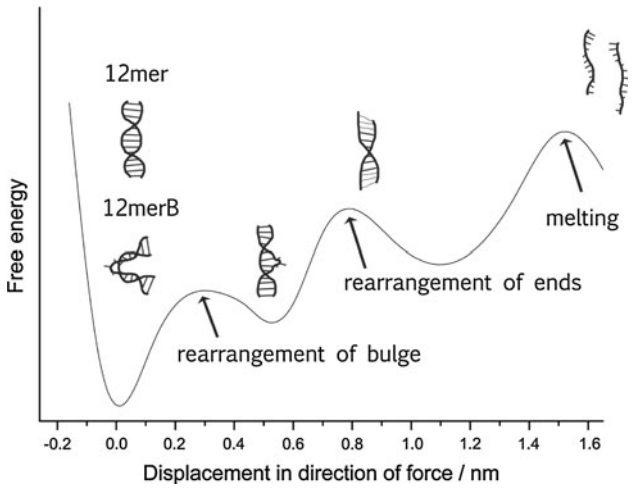

Fig. 5 Energy landscape view of force-induced dissociation. Force applied across the ends of the 12mer duplex and the 12mer duplex containing the UCU bulge (12merB) accelerates dissociation along the pathway proposed. The duplex containing the bulge undergoes a rearrangement via a transition state located at 0.38 nm. Rearrangement of the ends and the commencement of fraying occur over a transition state at 0.74 nm. Fraying of the GCG ends of the central poly(A)-tract containing sequence tested here is the dominant barrier under force and on traversing leads to rapid melting over the outer barrier

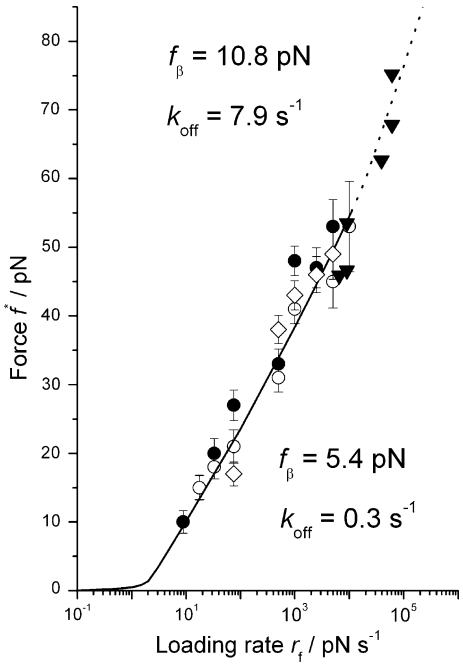

Fig. 6 Comparison of dynamic force data for the dissociation of the tri-nucleotide bulge duplex. The most probable rupture force f^* measured at loading rates between 10^1 and 10^4 pN s^{-1} obtained using the BFP are shown as *diamonds* (PBS buffer) and *circles* (HEPES buffer), and at loading rates between 10^4 and 10^5 pN s^{-1} obtained using the AFM are shown as *triangles* (Tris buffer). *Closed symbols* indicate the presence of magnesium. Also shown as the *solid and dotted line* is the predicted dynamic force spectrum for dissociation across a landscape containing two transition states: The inner transition state is characterized by a force scale $f_\beta = 10.8$ pN ($x_\beta = 0.4$ nm) and a dissociation rate $k_{off} = 7.9$ s^{-1} taken from the previous AFM study (Green et al. 2004); the outer transition state by a force scale $f_\beta = 5.4$ pN ($x_\beta = 0.8$ nm) and a dissociation rate $k_{off} = 0.3$ s^{-1}

by Strunz. We suggest, therefore, that this barrier is caused by the fraying of the CGC ends in the duplex, which is rate-limiting for the A_6-tract RNA and DNA under the forces measured, but is not the dominant barrier for random GC-content strands. In melting of non-poly(A) strands this barrier has to be overcome (the ends fray) before the denaturation bubbles and the critical nucleus form, and hence may be the origin of the 0.7 nm offset seen by Strunz.

The dynamic force data measured here using the BFP for the 12mer containing the UCU bulge reveal a force scale of 6.5 pN and an off-rate of 0.3 s^{-1}, and the dynamic force spectrum is indistinguishable from that measured for the non-bulge 12mer under the same conditions. The presence of the central bulge has not affected the dynamic force spectrum measured using the BFP. This result is consistent with our view of the dissociation process above and gives further support to the interpretation that the 0.6 nm/0.3 s^{-1} barrier is due to the fraying of the CGC ends, which are present and identical in both systems. The presence of the bulge would have, presumably, affected the formation of denaturation bubbles and the critical nucleus but because, at the 10^1 to 10^4 pN s^{-1} loading rates adopted here, we were not measuring the barrier to strand dissociation, only that of end fraying, our measurements were not affected by its presence.

An RNA duplex can be stabilized by the presence of magnesium ions in specific binding pockets within the molecule, and such a binding site is present within the UCU bulge (Serra et al. 2002). With a force scale of 6.9 pN and extrapolated off-rate of 0.3 s^{-1} our measurements of the force-induced melting of the 12mer containing the bulge in the presence of magnesium ions were identical with those taken without magnesium for the 12mer alone. This also supports the conclusion that our BFP measurements were probing an energy barrier to strand fraying, because the CGC pairing of the strand ends should not be affected by the presence of magnesium.

The BFP data for the 12mer with and without the tri-nucleotide bulge and with and without the presence of magnesium ions, and comparison with previously published data for both this RNA system and for DNA, leads us to believe that there is a transition state approximately 0.7 nm along the force-induced denaturation pathway caused by rearrangement and subsequent fraying of the ends of the duplex. Under the loading rates available to the BFP this energy barrier dominates in this RNA duplex containing the central poly(A) tract (Fig. 5). For more

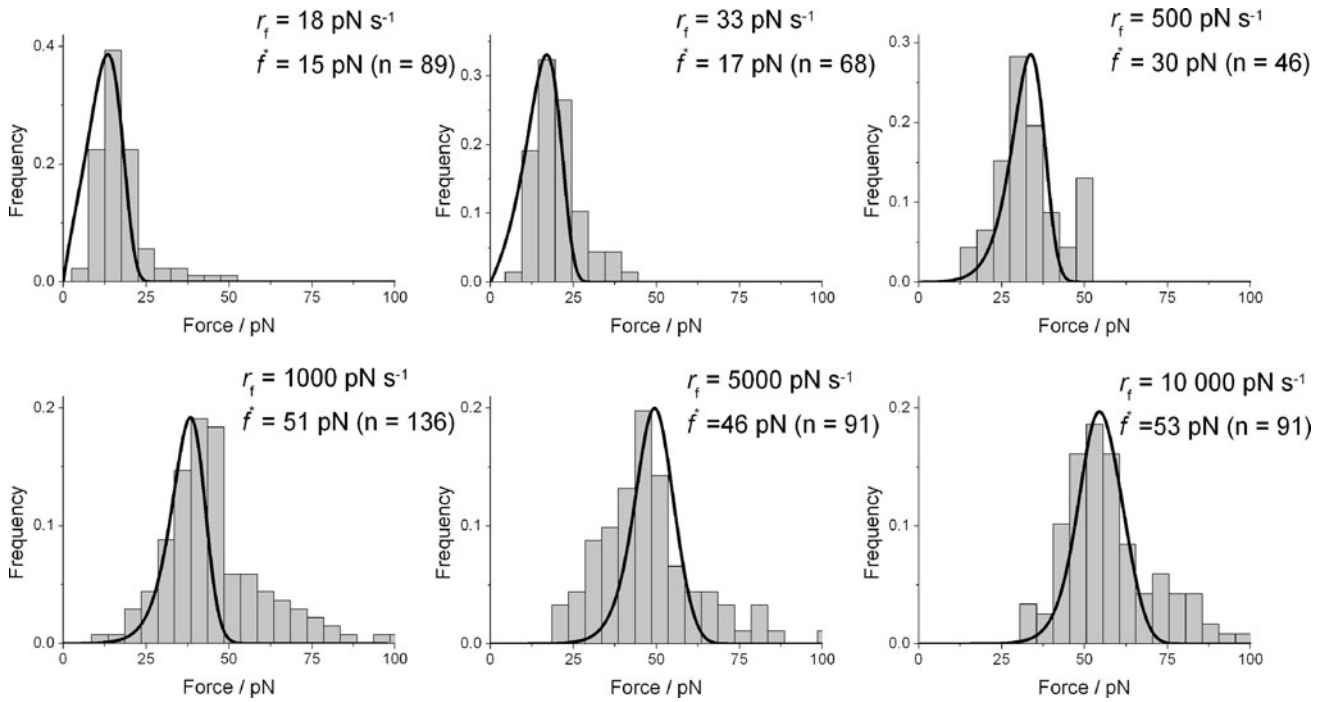

Fig. 7 Comparison of the measured force histograms with the predicted probability distributions at loading rates of 18, 33, 500, 1,000, 5,000, and 10,000 pN s^{-1} for measurements of the dissociation of 12mer-B in HEPES without magnesium. The probability distributions were calculated for the two-barrier system ($f_\beta = 10.8$ pN, $k_{off} = 7.9$ s^{-1} and $f_\beta = 5.4$ pN, $k_{off} = 0.3$ s^{-1}) by solving the corresponding kinetic master equations (Evans and Williams 2001; Williams et al. 2003)

stable duplexes (those with random sequence and central GC pairs forming the critical condensation nucleus) this energy barrier may not be seen until very high loading rates are used but is inferred from the 0.7 nm offset of the dominant barrier measured by Strunz et al. (1999). The relatively high loading rate in AFM force spectroscopy of the 12mer containing the bulge revealed a location different from the unfolding transition state characterized by a force scale of 10.8 pN and an off-rate of 7.9 s^{-1}. This transition state was only seen in this bulge containing sequence and not in the 12mer duplex. This study, showing the presence of the 7 pN barrier, supports the conclusion of our previous study that incorporation of the UCU bulge motif introduces an additional energy barrier into the force-induced denaturation landscape. This barrier is probably of a structural rearrangement, possibly straightening, of the bulge-containing duplex under force. Figure 6 shows the dynamic force data of the 12merB dissociation measured using the BPF in PBS and HEPES buffers with and without magnesium and measured using the AFM in Tris buffer. The solid and dotted line in Fig. 6 is the predicted dynamic force spectrum for the crossing of two energy barriers with force scales $f_\beta = 10.8$ pN ($x_\beta = 0.4$ nm), as published previously (Green et al. 2004), and $f_\beta = 5.4$ pN ($x_\beta = 0.8$ nm). The limited dynamic range of the AFM is clearly evident and further experimentation is required at loading rates higher than 10^5 pN s^{-1}, undertaken in the same buffer environment, to confirm the presence of these two barriers. It should also be noted that here no correction of the forces due to the significantly different hydrodynamic effects between the BFP and AFM has been made, and if done would serve to increase the difference between the two force scales measured.

Comparison of the histograms of forces measured at each loading rate with the distribution of forces predicted from the two-barrier model shows agreement is reasonable but suggests that some of the force histograms suffer from multiple and/or non-specific interactions (Fig. 7). Only by measuring hundreds, if not thousands, of forces and after full and accurate accounting for instrumental noise, hydrodynamic effects, finite sampling rates, and other factors, can the force histogram be used to infer more about dynamic force behaviour not seen in the spectrum (Williams 2008).

In the previous work with the AFM we studied a 24mer duplex d(CGCA$_{18}$CGC) with and without the bulge in addition to the 12mer studied here (Green et al. 2004). We measured one energy barrier for the 24mer characterized by a force scale of 7.0 ± 1.4 pN and an off-rate between 1 and 20 s^{-1}. The barrier location is identical with that found here of strand fraying, which is in agreement with what we now expect from this study, although the rate is faster. It seems that the increase in the length of the poly(A)-tract in the 24mer reduces the stability of the CGC-paired ends,

which is possibly an entropic effect, because of the increased length, although clearly more experiments are required to study this and the kinetics of the fraying. The AFM study of the 24mer with the central UCU bulge stabilized by magnesium revealed a barrier of force scale 2.8 pN and an off-rate of 10^{-4} s^{-1}. Intriguingly, at 1.5 nm this barrier location is the same as that predicted by Strunz for the dissociation of a 12-mer, and it would be interesting to study any dependence of the position of the bulge within the duplex on the melting transition state location. Removing the magnesium stabilization of the bulge returned the dynamic force spectrum of the 24mer bulge to that of the 24mer duplex (force scale 7.7 ± 0.3 pN, off-rate 10^{1} s^{-1}); that we can now attribute to measurement of GCG strand-end fraying.

Conclusions

By application of the biomembrane force probe for dynamic force spectroscopy we have been able to extend the view of the energy landscape for double-stranded RNA oligonucleotide dissociation events. The energy landscape revealed agrees with the view that fraying of the duplex ends precedes melting and is marked by an energy barrier 0.7 nm along the forced dissociation pathway. Duplexes with central poly(A)-tracts, such as those studied here, dissociate rapidly on melting of the ends. The investigation also confirms the prediction of a previous AFM-based study of the formation of a new transition state on introduction of a central UCU bulge.

References

Alcaraz J, Buscemi L, Puig-de-Morales M, Colchero J, Baro A, Navajas D (2002) Correction of microrheological measurements of soft samples with atomic force microscopy for the hydrodynamic drag on the cantilever. Langmuir 18:716–721

Bayas MV, Leung A, Evans E, Leckband D (2006) Lifetime measurements reveal kinetic differences between homophilic cadherin bonds. Biophys J 90:1385–1395

Braunlin WH, Bloomfield VA (1991) H-1-NMR study of the base-pairing reactions of D(GGAATTCC)—salt effects on the equilibria and kinetics of strand association. Biochemistry 30:754–758

Chen W, Evans EA, McEver RP, Zhu C (2008a) Monitoring receptor-ligand interactions between surfaces by thermal fluctuations. Biophys J 94:694–701

Chen W, Zarnitsyna VI, Sarangapani KK, Huang J, Zhu C (2008b) Measuring receptor-ligand binding kinetics on cell surfaces: from adhesion frequency to thermal fluctuation methods. Cell Mol Bioeng 1:276–288

Craig ME, Crothers DM, Doty P (1971) Relaxation kinetics of dimer formation by self complementary oligonucleotides. J Mol Biol 62:383

Dudko OK, Hummer G, Szabo A (2008) Theory, analysis, and interpretation of single-molecule force spectroscopy experiments. Proc Natl Acad Sci USA 105:15755–15760

Evans E (1998) Energy landscapes of biomolecular adhesion and receptor anchoring at interfaces explored with dynamic force spectroscopy. Faraday Discuss 111:1–16

Evans E (2001) Probing the relation between force—Lifetime—and chemistry in single molecular bonds. Annu Rev Biophys Biomol Struct 30:105–128

Evans E, Ritchie K (1997) Dynamic strength of molecular adhesion bonds. Biophys J 72:1541–1555

Evans E, Williams PM (2001) Dynamic force spectroscopy: 1. single bonds. In: Flyvberg H, Julicher F, Ormos P, David F (eds) Physics of bio-molecules and cells: Les houches session LXXV, 2–27 July 2001. Springer-Verlag, New York, pp 145–186

Evans E, Ritchie K, Merkel R (1995) Sensitive force technique to probe molecular adhesion and structural linkages at biological interfaces. Biophys J 68:2580–2587

Evans E, Leung A, Hammer D, Simon S (2001) Chemically distinct transition states govern rapid dissociation of single L-selectin bonds under force. Proc Natl Acad Sci USA 98:3784–3789

Evans E, Heinrich V, Leung A, Ieee II (2002) Receptor-cytoskeletal unbinding—In detachment of P-selectin from PSGL-1 on leukocytes Second Joint Embs-Bmes Conference 2002, vols 1–3, Conference Proceedings—bioengineering—integrative methodologies, New Technologies, pp 580–581

Evans E, Leung A, Heinrich V, Zhu C (2004) Mechanical switching and coupling between two dissociation pathways in a P-selectin adhesion bond. Proc Natl Acad Sci USA 101:11281–11286

Evans E, Heinrich V, Leung A, Kinoshita K (2005) Nano- to microscale dynamics of P-selectin detachment from leukocyte interfaces. I. Membrane separation from the cytoskeleton. Biophys J 88:2288–2298

Evans E, Kinoshita K, Simon S, Leung A (2010) Long-lived, high-strength states of ICAM-1 bonds to beta(2) integrin, I: lifetimes of bonds to recombinant alpha(L) beta(2) under force. Biophys J 98:1458–1466

Galligan E, Roberts CJ, Davies MC, Tendler SJB, Williams PM (2001) Simulating the dynamic strength of molecular interactions. J Chem Phys 114:3208–3214

Gourier C, Jegou A, Husson J, Pincet F (2008) A nanospring named erythrocyte. The biomembrane force probe. Cell Mol Bioeng 1:263–275

Grange W, Strunz T, Schumakovitch I, Guntherodt HJ, Hegner M (2001) Molecular recognition and adhesion of individual DNA strands studied by dynamic force microscopy. Single Mol 2:75–78

Green NH, Williams PM, Wahab O, Davies MC, Roberts CJ, Tendler SJB, Allen S (2004) Single-molecule investigations of RNA dissociation. Biophys J 86:3811–3821

Guerriertakada C, Altman S (1984) Catalytic activity of an RNA molecule prepared by transcription in vitro. Science 223:285–286

Harris SA, Sands ZA, Laughton CA (2005) Molecular dynamics simulations of duplex stretching reveal the importance of entropy in determining the biomechanical properties of DNA. Biophys J 88:1684–1691

Heinrich V, Ounkomol C (2007) Force versus axial deflection of pipette-aspirated closed membranes. Biophys J 93:363–372

Heinrich V, Leung A, Evans E (2005) Nano- to microscale dynamics of P-selectin detachment from leukocyte interfaces. II. Tether flow terminated by P-selectin dissociation from PSGL-1. Biophys J 88:2299–2308

Hummer G, Szabo A (2003) Kinetics from nonequilibrium single-molecule pulling experiments. Biophys J 85:5–15

Janovjak H, Struckmeier J, Muller DJ (2005) Hydrodynamic effects in fast AFM single-molecule force measurements. Eur Biophys J Biophys Lett 34:91–96

Kinoshita K, Leung A, Simon S, Evans E (2010) Long-lived, high-strength states of ICAM-1 bonds to beta(2) integrin, II: lifetimes of LFA-1 bonds under force in leukocyte signaling. Biophys J 98:1467–1475

Maali A, Hurth C, Boisgard R, Jai C, Cohen-Bouhacina T, Aime JP (2005) Hydrodynamics of oscillating atomic force microscopy cantilevers in viscous fluids. J Appl Phys 97:6

Merkel R, Nassoy P, Leung A, Ritchie K, Evans E (1999) Energy landscapes of receptor-ligand bonds explored with dynamic force spectroscopy. Nature 397:50–53

Moore A, Williams PM, Davies MC, Jackson DE, Roberts CJ, Tendler SJB (1998) Enthalpic approach to the analysis of the scanning force ligand rupture experiment. J Chem Soc Perkin Trans 2:253–258

Moore A, Williams PM, Davies MC, Jackson DE, Roberts CJ, Tendler SJB (1999) Analyzing the origins of receptor-ligand adhesion forces measured by the scanning force microscope. J Chem Soc Perkin Trans 2:419–423

Patel AB, Allen S, Davies MC, Roberts CJ, Tendler SJB, Williams PM (2004) Influence of architecture on the kinetic stability of molecular assemblies. J Am Chem Soc 126:1318–1319

Perret E, Leung A, Feracci H, Evans E (2004) Trans-bonded pairs of E-cadherin exhibit a remarkable hierarchy of mechanical strengths. Proc Natl Acad Sci USA 101:16472–16477

Pope LH, Davies MC, Laughton CA, Roberts CJ, Tendler SJB, Williams PM (2001) Force-induced melting of a short DNA double helix. Eur Biophys J Biophys Lett 30:53–62

Porschke D (1971) Cooperative nonenzymic base recognition.2. thermodynamics of helix-coil transition of oligoadenylic and oligouridylic acids. Biopolymers 10:1989

Porschke D, Eigen M (1971) Co-operative non-enzymic base recognition.3. kinetics of helix-coil transition of oligoribouridylic oligoriboadenylic acid system and of oligoriboadenylic acid aloe at acidic pH. J Mol Biol 62:361

Porschke D, Uhlenbec OC, Martin FH (1973) Thermodynamics and kinetics of helix–coil transition of oligomers containing GC base pairs. Biopolymers 12:1313–1335

Schumakovitch I, Grange W, Strunz T, Bertoncini P, Guntherodt HJ, Hegner M (2002) Temperature dependence of unbinding forces between complementary DNA strands. Biophys J 82:517–521

Serra MJ, Baird JD, Dale T, Fey BL, Retatagos K, Westhof E (2002) Effects of magnesium ions on the stabilization of RNA oligomers of defined structures. RNA Publ RNA Soc 8:307–323

Simson DA, Ziemann F, Strigl M, Merkel R (1998) Micropipet-based pico force transducer: in depth analysis and experimental verification. Biophys J 74:2080–2088

Sinha ND, Biernat J, McManus J, Koster H (1984) Polymer support oligonucleotide synthesis.18. Use of beta-cyanoethyl-*N*,*N*-dialkylamino-*N*-morpholino phosphoramidite of deoxynucleosides for the synthesis of DNA fragments simplifying deprotection and isolation of the final product. Nucleic Acids Res 12:4539–4557

Strunz T, Oroszlan K, Schafer R, Guntherodt HJ (1999) Dynamic force spectroscopy of single DNA molecules. Proc Natl Acad Sci USA 96:11277–11282

Williams PM (2003) Analytical descriptions of dynamic force spectroscopy: behaviour of multiple connections. Anal Chim Acta 479:107–115

Williams PM (2006) Force Spectroscopy. In: Samori P (ed) Scanning probe microscopies: beyond imaging. Wiley–VCH, Weinheim, pp 250–274

Williams PM (2008) Dynamic force spectroscopy with the atomic force microscope. In: Noy A (ed) Handbook of molecular force spectroscopy. Springer, New York, pp 142–160

Williams AP, Longfellow CE, Freier SM, Kierzek R, Turner DH (1989) Laser temperature-jump, spectroscopic, and thermodynamic study of salt effects on duplex formation by DGCATGC. Biochemistry 28:4283–4291

Williams PM, Moore A, Stevens MM, Allen S, Davies MC, Roberts CJ, Tendler SJB (2000) On the dynamic behaviour of the forced dissociation of ligand-receptor pairs. J Chem Soc Perkin Trans 2:5–8

Williams PM, Fowler SB, Best RB, Toca-Herrera JL, Scott KA, Steward A, Clarke J (2003) Hidden complexity in the mechanical properties of titin. Nature 422:446–449